Journal of the Optical Society of America B
OPTICAL PHYSICS

Infrared diffraction radiation from twin circular dielectric rods covered with graphene: plasmon resonances and beam position sensing

Dariia O. Herasymova,* Sergii V. Dukhopelnykov, and Alexander I. Nosich

Laboratory of Micro and Nano Optics, Institute of Radio-Physics and Electronics NASU, Kharkiv, Ukraine
**Corresponding author: dariia.heras@gmail.com*

Received 19 April 2021; revised 12 July 2021; accepted 18 July 2021; posted 20 July 2021 (Doc. ID 428037); published 17 August 2021

This work considers the near-infrared range diffraction radiation (DR) from a modulated beam of particles passing between two identical dielectric circular nanowires covered with graphene. The resistive boundary conditions are set on the zero-thickness graphene covers with the electron conductivity determined from the Kubo formalism. Assuming that the beam velocity is fixed, we use the separation of variables in local coordinates and the addition theorems for cylindrical functions and cast the DR problem to a Fredholm second-kind matrix equation. This allows us to compute both near- and far-field characteristics with controlled accuracy. The analysis reveals that a shift of the beam trajectory from the central-symmetric position enables the excitation of additional resonances on the modes, which remain "dark" otherwise. Ignition of these resonances can be considered as a tool for noninvasive beam position monitoring with microscale devices.

https://doi.org/10.1364/JOSAB.428037

1. INTRODUCTION

Graphene is a new material that consists of a monolayer or a few such layers of graphite, i.e., has subnanometer thickness. It has remarkable properties like transparency in the visible range, mechanical strength, and good electron conductivity in the terahertz and infrared (IR) ranges. The conductivity is a function of the temperature, electron relaxation time, frequency, and chemical doping. Graphene can support the plasmon-guided wave at the terahertz and IR frequencies that makes its electromagnetic properties similar to noble metal ones in the visible-light range, but at much lower frequencies. What is principally new is that graphene conductivity and hence the plasmon effect can be tuned using the DC bias, which translates to the chemical potential [1,2]. Usually, graphene is attached to flat dielectric substrates; however, now curved substrates have been attracting increasing attention [3,4]. Recently, graphene-covered nanowire fabrication and synchrotron nanospectroscopy measurements have been reported in [5]. Note that circular-wire dimers coated with graphene have been studied with commercial codes in the context of field forces [6] and cloaking [7], and with in-house code based on the local Fourier expansions in the analysis of eigenfrequencies [8].

Diffraction radiation (DR) is a term used to characterize the effect of the electromagnetic-wave radiation, of any frequency that accompanies the electron beams flowing near metal and dielectric objects. An early example of DR is the Smith–Purcell effect [4], or visible-light radiation from the electron beam moving across a grating. Later it was extensively studied theoretically in [9–12] and other publications. As DR is the radiation of the currents induced by the beam, on the nearby metal and dielectric scatterers, it perfectly matches the design requirements of noninvasive beam position monitors (BPMs).

Microwave-range BPMs are already in use at probably all existing accelerators and colliders [13–17]. The nanoscale circuit elements, available today due to the progress of nanotechnology, open new opportunities in the design of BPMs based on terahertz, IR, visible-light, and ultraviolet range DR [18–27].

The small size of micro- and nanosized scatterers makes their effect on the beam velocity and trajectory negligible, so that one can consider these parameters as fixed. Then, the modeling of the DR effect can be performed using linear formulation, as a problem of classical electromagnetic-wave scattering theory. However, unlike conventional plane or spherical waves, the incident wave, which produces DR, is the given field of a charged particle or a beam in free space. In the latter case, such a field is a slow wave, traveling with the same phase velocity as the beam itself. What is especially interesting is that this field is antisymmetric with respect to the beam trajectory.

Measuring the DR intensity in the near or far zone, one can monitor the electron-beam parameters. As BPM is a specific sensor, optimization of its performance requires finding a favorable combination of its elements' shapes and materials. Here, the use the resonance effects is a promising approach. A resonance enhances the DR intensity proportionally to the associated Q-factor of the resonating mode. In the microwave range,

various coaxial metallic hollow cavities integrated with the drift tubes are common. This approach can be extended to the terahertz and IR ranges if suitable resonators shaped as subwavelength scatterers are found. One possible approach is the use of high-refractive-index materials; however, available today dielectric materials have refractive indices within several dozens, so that the resonances on their lowest modes entail only moderately subwavelength dimensions [23,24]. The other approach uses the noble-metal scatterers, able to support the surface plasmon modes in the visible range; however, these modes have rather low Q-factors [25,26]. The way out can be seen in the exploitation of the plasmon modes on the patterned graphene or graphene-coated scatterers. Note that such configurations have already been studied as the elements of promising IR and terahertz range sensors of the host-medium refractive index [28] and tunable filers [29,30], absorbers [31], scatterers [32], and antennas [33].

The Q-factors of the graphene plasmon modes in the terahertz and IR ranges have moderate values (20–100) that are higher than those of a solid metal wire in the visible-light range. This makes graphene-coated dielectric micro- and nanowires attractive as resonance scatterers in many applications [1–8], including DR-based BPMs.

In the case of 2D modeling, the design of a DR-based BPM sensor must involve not a single scatterer but two identical ones, for instance, the edges of a slot [19], so that the beam moves between them. Then a difference in the DR intensity or in the angular radiation patterns from the opposite sides of the beam trajectory can serve as indicator of a shift in the beam position. This explains the interest in the twin solid dielectric nanowire and twin noble-metal solid-wire and nanotube BPM configurations, studied numerically in [23–26], respectively. DR from a dimer of spherical dielectric particles has been studied in [27] in an approximate manner, using the concept of the averaged polarizability.

In this work, we study an IR-range BPM configuration, based on twin dielectric nanowires coated with graphene covers (see Fig. 1). In our full-wave analysis, we follow that of [24–26], modified to account for the graphene coating. Our goal is to investigate how the position of the beam trajectory influences the power of DR and the excitation of high-Q plasmon resonances.

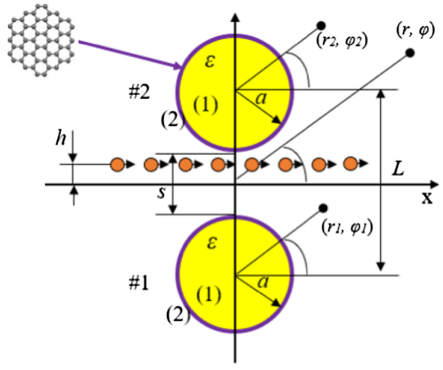

Fig. 1. Cross-sectional geometry of electron beam moving between a pair of identical dielectric circular microwires with graphene covers.

2. PROBLEM FORMULATION AND BASIC EQUATIONS

We consider a flat zero-thickness beam of electrons flowing along the straight trajectory at the distance h from the x axis, with a fixed velocity $v = \beta c$, where c is the light velocity and $\beta < 1$. The beam charge density function, if modulated in time in harmonic manner with the frequency ω and amplitude ρ_0, is

$$\rho = \rho_0 \delta(y - h) \exp[i(kx/\beta - \omega t)], \tag{1}$$

where $\delta(\cdot)$ is the Dirac delta function and $k = \omega/c$ is the free-space wavenumber. Note that the harmonically modulated beam charge [Eq. (1)] can be associated with the Fourier transform, in time, of the charge of single particle. Besides, the beam charge density can be premodulated using a periodic waveguide or external laser illumination [21].

As is known (see [10–13], for instance), the field of the beam [Eq. (1)] is an H-polarized slow surface wave propagating along the beam trajectory with the same phase velocity as the beam itself,

$$H_z^0(x, y) = A\beta \,\mathrm{sign}(y - h) e^{-q|y-h|} e^{i(k/\beta)x}, \tag{2}$$

where $q = k\gamma/\beta$, $\gamma = (1 - \beta^2)^{1/2}$ is inverse Lorentz factor, $\mathrm{sign}(\cdot) = \pm 1$, the time dependence is omitted, and the constant in the SI system of units is $A = c\rho_0/2$.

Figure 1 presents the considered BPM configuration. Two identical circular dielectric wires with graphene covers (marked #1 and #2) have the radius a and refractive index $\alpha = \sqrt{\varepsilon}$. They are placed in the free space with the air gap s, and L is the distance between their axes. We assume that the modulated beam of particles [Eq. (1)] flies in parallel to the x direction between the wires at the distance h from the center of the air gap. We introduce the Cartesian and the local $(r_{1,2}, \varphi_{1,2})$ and global (r, φ) polar coordinates, as shown in Fig. 1. The formulation of the 2D wave-scattering boundary-value problem involves the Helmholtz equation with corresponding wavenumber in each partial domain, the graphene-surface boundary conditions at the wire contours, the Sommerfeld radiation condition at infinity, and the condition of local power finiteness. These conditions guarantee the uniqueness of the boundary-value problem solution.

In the case of H-polarization, one can derive all the field components from the z component of the magnetic field vector. Omitting the index z, we look for the total field as follows:

$$H_z^{\mathrm{tot}} = \begin{cases} H_z^{\mathrm{int}(p)}, & r_p < a_p, \quad p = 1, 2 \\ H_z^0 + H_z^{\mathrm{ext}}, & r_p > a_p \end{cases} \tag{3}$$

Inside each wire and off them (domains (1) and (2)), we expand the field in the azimuthal Fourier series in the local polar coordinates, respectively, so that

$$H_z^{\mathrm{int}(p)}(r, \varphi) = \sum_{n=-\infty}^{\infty} y_n^{(p)} J_n(k\alpha r_p) e^{in\varphi_p}, \quad r_p < a, \quad p = 1, 2, \tag{4}$$

$$H_z^{\mathrm{ext}}(r, \varphi) = \sum_{p=1,2} \sum_{n=-\infty}^{\infty} z_n^{(p)} H_n(k r_p) e^{in\varphi_p}, \quad r_p > a, \tag{5}$$

where $y_n^{(p)}$ and $z_n^{(p)}$ $(n=0,\pm1,\pm2,\ldots,\ p=1,2)$ are unknown coefficients and $H_m(\cdot)$ and $J_m(\cdot)$ are the Hankel (first kind) and the Bessel functions, respectively. Note that expressions (4) and (5) satisfy the Helmholtz equation, the radiation condition, and the local power finiteness condition in term-wise manner.

The boundary conditions at the wire contours, $r_p=a$, $0\le\varphi_p<2\pi$ $(p=1,2)$, are the conditions for a zero-thickness resistive sheet placed at the interface between the free space and dielectric—see, e.g., [34] for details. They are two: one tells that the tangential electric field should be continuous across the coated wire contour,

$$E_{\varphi_p}^{\mathrm{int}(p)}=E_{\varphi_p}^{0}+E_{\varphi_p}^{\mathrm{ext}}, \tag{6}$$

and the other tells that the tangential magnetic field has a jump proportional to the surface conductivity of graphene,

$$E_{\varphi_p}^{\mathrm{int}(p)}+E_{\varphi_p}^{0}+E_{\varphi_p}^{\mathrm{ext}}=2ZZ_0\left[H_z^{\mathrm{int}(p)}-H_z^{0}-H_z^{\mathrm{ext}}\right]. \tag{7}$$

Here, the graphene complex-valued surface impedance in the terahertz range (where the interband conductivity can be safely neglected [1–3,34]) is

$$Z_0Z(\omega,\mu_c,\tau,T)=1/\sigma_{\mathrm{intra}}, \tag{8}$$

where $Z_0=\sqrt{\mu_0/\varepsilon_0}$ is the free-space impedance, Z is the normalized impedance, and σ_{intra} is the intraband surface conductivity, also known as the Drude model. The latter quantity is found from the Kubo formalism as [34]

$$\sigma_{\mathrm{intra}}=\frac{iq_e^2k_BT}{\pi\hbar^2\left(\omega+i\tau^{-1}\right)}\left[\frac{\mu_c}{k_BT}+2\ln\left(1+e^{-\frac{\mu_c}{k_BT}}\right)\right], \tag{9}$$

where q_e is the electron charge, k_B is the Boltzmann constant, T is the temperature, $\hbar$ is the reduced Planck constant, τ is the electron relaxation time, and μ_c is the chemical potential.

Our treatment of the formulated above boundary-value problem follows all steps of the preceding papers [24–26], where the dimers of bare dielectric and silver wires and silver tubes were considered, respectively, excited by a modulated electron beam. The difference is in the boundary condition [Eq. (7)], which now involves the graphene parameters. Therefore, we omit the details of the derivations which can be found in [24–26].

On expanding the beam field [Eq. (2)] in terms of the Fourier series in the local coordinates [10],

$$H_z^0(r_{1,2},\varphi_{1,2})=\mp A\beta e^{-q(L/2\pm h)}\times\sum_{m=-\infty}^{+\infty}i^mJ_m(kr_{1,2})\left(\frac{1\mp\gamma}{\beta}\right)^m e^{im\varphi_{1,2}}, \tag{10}$$

we substitute the series (4), (5), and (10) into the conditions (6) and (7) and use the Graf addition theorem for the cylindrical functions to transfer the expansions from one local coordinate system to the other, similar to [24–26]. Finally, on introducing new unknowns, $z_n^{(p)}=x_n^{(p)}w_n$, $w_{n>0}=n!(2/ka)^{2n}$, $w_{n<0}=(-1)^nw_{n>0}$, we derive coupled infinite-matrix equations $(p\ne j=1,2)$,

$$x_m^{(p)}+\frac{V_m}{D_m}\sum_{n=-\infty}^{+\infty}(\pm i)^{n-m}w_nH_{m-n}(kL)x_n^{(j)}=\frac{F_m^{(p)}}{D_m},\quad m=0,\pm1,\pm2,\ldots, \tag{11}$$

where

$$V_m=iZ^{-1}J_m'(ka)J_m'(k\alpha a)+\alpha J_m'(ka)J_m(k\alpha a)-J_m(ka)J_m'(k\alpha a), \tag{12}$$

$$D_m=w_m\left[iZ^{-1}H'_m(ka)J'_m(k\alpha a)+\alpha H'_m(ka)J_m(k\alpha a)-H_m(ka)J'_m(k\alpha a)\right], \tag{13}$$

$$F_m^{(p)}=-iZ^{-1}f_m'^{(p)}J_m'(k\alpha a)-f_m'^{(p)}\alpha J_m(k\alpha a)-f_m^{(p)}J_m'(k\alpha a), \tag{14}$$

$$f_m^{(1,2)}=\mp Ae^{-q(L/2\pm h)}i^mJ_m(ka)(1\mp\gamma)^m\beta^{-m+1},\qquad f_m'^{(1,2)}=\partial f_m^{(1,2)}/\partial(ka). \tag{15}$$

What is important is that, thanks to the rescaling of the unknowns with the aid of the factors w_n, the matrix Eq. (11) is the Fredholm second-kind operator equation provided that $L>2a$ (see the explanations in [24–26]; note that here the presence of the terms with Z^{-1} does not spoil this property). This guarantees the convergence of the numerical solution of Eq. (11), in the mathematical sense: if each block of Eq. (11) is truncated to finite order N, then, by taking progressively larger values of N, one can minimize the error in finding the coefficients $\{x_m^{(1,2)}\}_{m=-N}^{+N}$, in principle, to machine precision. Note that without the mentioned rescaling, the matrix equation of this kind can provide, at best, the accurate values of the first two to three digits and hence remains impractical in the case of sharp resonances. This crucial circumstance is frequently overlooked or neglected, even in the tutorials; see, for instance, [8,35–38].

As we are interested in the modeling of BPM, we have to compute some DR characteristics, which can be observable in practical situations. As usual, such characteristics are related to the field far from the scatterers.

On substituting into Eq. (5) the expressions for the Hankel functions of the large argument, $H_n(x)\sim(2/i\pi x)^{1/2}(-i)^n\exp(ix)$, we see that the field at $r\to\infty$ is the cylindrical wave,

$$H_z^{\mathrm{sc}}(r,\varphi)=\left(\frac{2}{i\pi kr}\right)^{1/2}\Phi(\varphi)e^{ikr}, \tag{16}$$

where the angular scattering pattern depends on $z_m^{(1,2)}$ as

$$\Phi(\varphi)=\sum_{m=-\infty}^{+\infty}(-i)^mJ_m(ka)\left[e^{-\frac{1}{2}ikL\sin\varphi}z_m^{(1)}+e^{\frac{1}{2}ikL\sin\varphi}z_m^{(2)}\right]e^{im\varphi}, \tag{17}$$

Then the partial scattering cross sections (SCSs) corresponding to the DR power, radiated to the lower and the upper half-spaces, are, respectively,

$$\sigma_{\mathrm{sc}}^{(1,2)}=\frac{2}{\pi kA^2}\int_0^{\pm\pi}|\Phi(\varphi)|^2\mathrm{d}\varphi. \tag{18}$$

Still, the scattering is accompanied with the absorption because graphene is a lossy material; see Eqs. (8) and (9). Therefore, we introduce the partial absorption cross sections (ACSs), found as

$$\sigma_{\text{abs}}^{(1,2)} = \pi a \frac{\text{Re}Z}{A^2|Z|} \sum_{n=-\infty}^{\infty} \left| f_n'^{(1,2)} + z_n^{(1,2)} H'_n(ka) + J'_n(ka) \sum_{m=-\infty}^{\infty} (\pm i)^{m-n} z_m^{(2,1)} H_{n-m}(kL) \right|^2. \quad (19)$$

Note that the sum of the partial SCS and ACS is the extinction cross section, $\sigma_{\text{ext}} = \sigma_{\text{sc}}^{(1)} + \sigma_{\text{sc}}^{(2)} + \sigma_{\text{abs}}^{(1)} + \sigma_{\text{abs}}^{(2)}$. This value is linked to the DR far-field amplitude [Eq. (17)], computed in the directions of the so-called complex angles of incidence (see [25] for details),

$$\sigma_{\text{ext}} = -\frac{4}{kA^2} e^{-qL/2} \text{Re} \sum_{m=-\infty}^{+\infty} (-i)^m \beta^m J_m(ka) \times \left[\frac{e^{-qh} z_m^{(1)}}{(1+\gamma)^m} + \frac{e^{qh} z_m^{(2)}}{(1-\gamma)^m} \right]. \quad (20)$$

This is the optical theorem for the DR, which accompanies the motion of the modulated beam of charged particles near obstacles. It can be used for a partial validation of the computed results. In our analysis, this expression has been satisfied at the level of machine precision.

3. NATURAL MODES OF GRAPHENE-COVERED DIELECTRIC WIRES

Each circular dielectric wire covered with graphene is a composite open resonator that supports the natural modes of two families: dielectric-rod modes, which obtain the features of the whispering-gallery (WG) modes if the radius a and/or refractive index a is getting larger, and the plasmon modes of the graphene cover.

On the stand-alone circular graphene-coated wire, complex frequencies of all natural modes satisfy independent equations $D_m = 0 (m = 0, 1, \ldots)$, where D_m is given by Eq. (13). The plasmon modes appear in every nonzero azimuthal order, $m = 1, 2, \ldots$ [21]. In [8], they have been found approximately, after using small-argument asymptotics in Eq. (13). However, by analogy to a silver wire [39], they can be also viewed as the natural modes of the traveling-wave resonator formed by the closed contour of the graphene cover. Then, neglecting the curvature of the graphene layer, the following empiric characteristic equation can be established:

$$\exp\left(i g_{\text{plasm}} 2\pi a\right) = 1, \quad (21)$$

where g_{plasm} is the complex wavenumber of the plasmon wave propagating along a flat infinite graphene monolayer located at the interface between air and dielectric. The roots of this equation are, obviously, $g_{\text{plas}} a = m$, $m = 1, 2, \ldots$ and correspond to the plasmon modes, P_m. The value of g_{plasm} can be found analytically; see Eq. (31) in [32],

$$g_{\text{plas}}^2 \approx -k^2(1+\varepsilon)\left[Z^2(1+\varepsilon) - \frac{1}{2} + O(|Z|^{-2}) \right]. \quad (22)$$

Taking into account that graphene's normalized surface impedance Z depends on the frequency [Eqs. (8) and (9)] and has large value in the terahertz and IR ranges, $|Z|^2 \gg 1$, we conclude that

$$g_{\text{plas}} \approx k^2(\varepsilon+1)\frac{c}{\Omega}\left(1 + \frac{i\tau^{-1}}{kc}\right), \quad (23)$$

where Ω is a constant that follows from Eq. (9), namely,

$$\Omega = \frac{q_e^2 Z_0 k_B T}{\pi \hbar^2} \left\{ \frac{\mu_c}{k_B T} + 2 \ln\left[1 + \exp\left(-\frac{\mu_c}{k_B T} \right) \right] \right\}. \quad (24)$$

Then, the plasmon mode P_m resonance frequencies are found approximately as

$$f_m^P \approx \frac{1}{2\pi} \left[\frac{mc\Omega}{a(\varepsilon+1)} \right]^{1/2}. \quad (25)$$

Note that expression (25) agrees with Eq. (12) of [8] [here, one has to account for the different systems of units, the centimeter–gram–second system of units (CGS) in [8] and SI in our work]. Besides, the Q-factors of the plasmon modes, in the same approximation (i.e., the absorption Q-factors) are found to be proportional to the electron relaxation time,

$$Q_m^P \approx \frac{4\varepsilon\tau}{(1+\varepsilon)^{3/2}} \left(\frac{mc\Omega}{a} \right)^{1/2}. \quad (26)$$

As one can see, both resonance frequencies and Q-factors of the plasmon modes of a graphene-covered circular dielectric wire grow as a square root of the mode index. Additionally, in view of Eq. (24), they grow approximately as a square root of the chemical potential, which, in its turn, is known to be proportional to DC bias. Therefore, higher-order plasmon modes have a certain advantage, in the higher Q-factors, before the lower-index modes, including the principal "dipole" mode, P_1. The growth with m is limited, however, by the radiation losses, which were neglected when deriving Eqs. (25) and (26). The spectral distance between the adjacent plasmon modes gets smaller with m and grows as a square root of the chemical potential.

The dielectric-wire modes, perturbed by the presence of graphene cover, also correspond to the (other) roots of equations $D_m = 0$; if $|Z| \gg 1$ and $m \gg ka \gg m/\alpha$, they obtain the features of the WG modes, such as periodically spaced frequencies and high Q-factors. However, due to the losses in graphene, the exponential growth of the Q-factors with m and α is now limited at the level, determined by the graphene parameters, τ, μ_c and T.

Note also that, in a stand-alone circular resonator, all modes with $m > 1$ are doubly degenerate, because $\sin m\varphi$ and $\cos m\varphi$ field dependences are orthogonal and lead to the identical characteristic equations.

However, the configuration of twin circular dielectric wires (Fig. 1), known as dimer, is an even more complicated open resonator because the modes of individual wires are now optically coupled. Mathematically, this is visible from the fact that now the mode equations do not split into the azimuthal orders, and their natural frequencies are the roots of the determinantal equation, generated by the whole matrix [Eq. (11)]. Physically, the optical coupling forces the modes to hybridize; to emphasize the coupling, the hybrid modes of the dimer are called "supermodes" [40]. Due to the presence of two lines of symmetry, in the cross section (which are the x and the y axes), all supermodes of a circular-wire dimer split into four orthogonal classes according to the field symmetry (even dependence) or antisymmetry (odd dependence) along these axes. They are usually denoted as *EE*, *EO*, *OE*, and *OO* classes and can be studied separately after the separation of corresponding determinantal equations [40].

Therefore, for a dimer of twin circular open resonators, instead of a single doubly degenerate mode of each wire, a quartet of closely spaced supermodes appears. A numerical study of the supermodes of twin dielectric disks has shown (see [40]) that each quartet of supermodes forms two even closer spaced doublets, of the *EE* and *OE* modes and the *EO* and *OO* modes, respectively. Recently, the same has been demonstrated for the supermodes of a dimer of graphene-covered dielectric wires [8].

4. NUMERICAL RESULTS

Figures 2–4 present the results of the calculation of normalized partial SCS and ACS versus the frequency for twin graphene-covered dielectric nanowires with radius $a = 500$ nm and 100 nm, separated by the air gap of the width $s = 100$ nm. The relative dielectric constant of the wire material is assumed to be 2.4. Graphene parameters are $T = 300°$K, $\tau = 0.5$ ps, and several values of the chemical potential are tried. Two beams with the same relative velocity $\beta = 0.5$ are considered: not shifted from the central-symmetric position, $h = 0$, and shifted by $h = 40$ nm.

The truncation order of the blocks of the matrix Eq. (12) is selected according to the rule, explained in [41]: $N = \max\{k\alpha a,\ ka/\beta\} + 5$, which guarantees five correct digits in the found coefficients. This rule is especially important for the nonrelativistic beams, $\beta \ll 1$, because the right-hand part

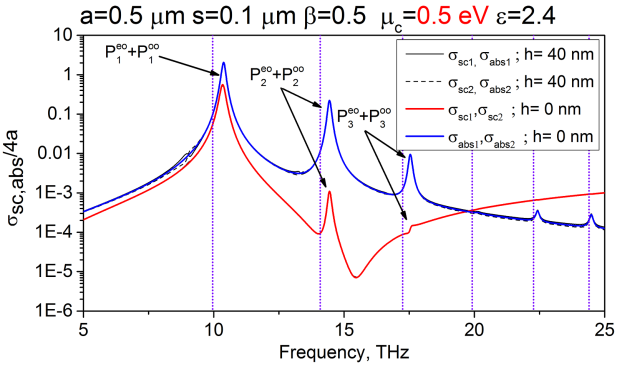

Fig. 2. Normalized partial SCS and ACS versus the frequency for twin dielectric nanowires covered with graphene with radius $a = 0.5$ μm, air gap $s = 0.1$ μm, chemical potential $\mu_c = 0.5$ eV, and beam shifts $h = 0$ and 40 nm. Dotted vertical lines are the single-wire plasmon-mode frequencies, predicted by Eq. (25).

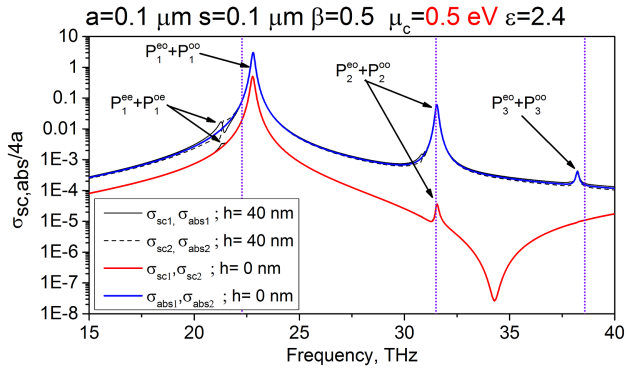

Fig. 3. Same as in Fig. 2 for the radius $a = 0.1$ μm.

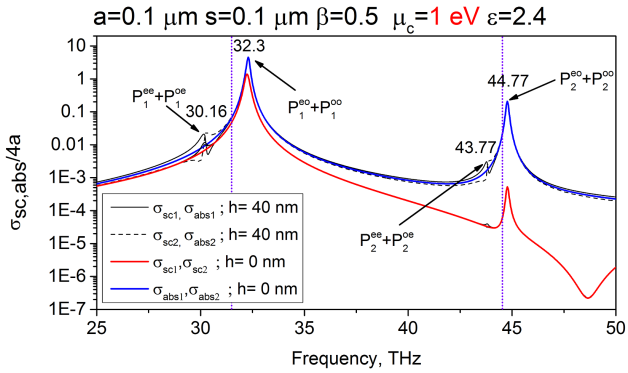

Fig. 4. Same as in Fig. 3 for the chemical potential $\mu_c = 1$ eV.

coefficients in Eq. (11) behave as $O[(ka/2\beta)^{|n|}]$ if $|n| > ka$, i.e., drop slowly.

For the selected geometrical and material parameters, single-wire plasmon-mode resonance frequencies are well predicted by Eq. (25) (see [32,33]) and get to the IR frequency range. Small shifts from Eq. (25), for the dimer supermodes, can be also estimated analytically; see [8].

As can be seen in Fig. 2, if the wire radius is $a = 500$ nm and graphene's chemical potential is $\mu_c = 0.5$ eV, there are a few lower-frequency plasmon-mode resonances both in the scattering and in the absorption. However, they are almost the same both with and without the shift of the beam trajectory from the central-symmetric position, where it passes through the air-gap center. This means that the supermodes of the twin-wire dimer that belong to the classes *EE* and *OE* ("dark" if the shift is absent) remain very weakly excited (see small bumps on the red side of Eq. (25), unlike their sister-modes of the *EO* and *OO* classes. The latter supermodes shine as one peak (i.e., are still unresolved) in both cases on the blue side of each frequency, predicted by Eq. (25).

This unfavorable factor for the BPM design situation can be overcome if the Q-factors of the plasmon supermodes are made larger. Equations (26) and (24) show that this can be achieved by either making the wire radius smaller or increasing the chemical potential of graphene, i.e., using a larger DC bias. This effect is accompanied with a frequency shift to higher values, see Eq. (25); it should still hold for the supermodes of each symmetry class.

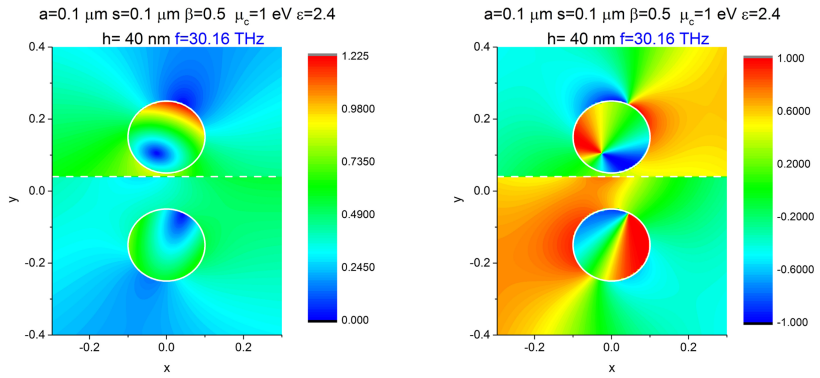

(a) 30.16 THz

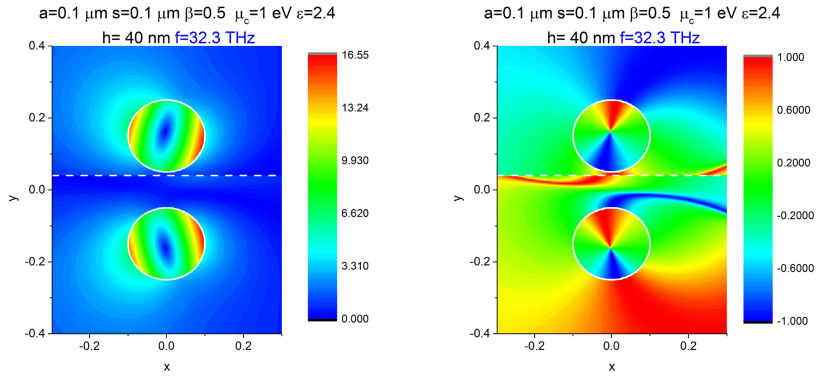

(b) 32.3 THz

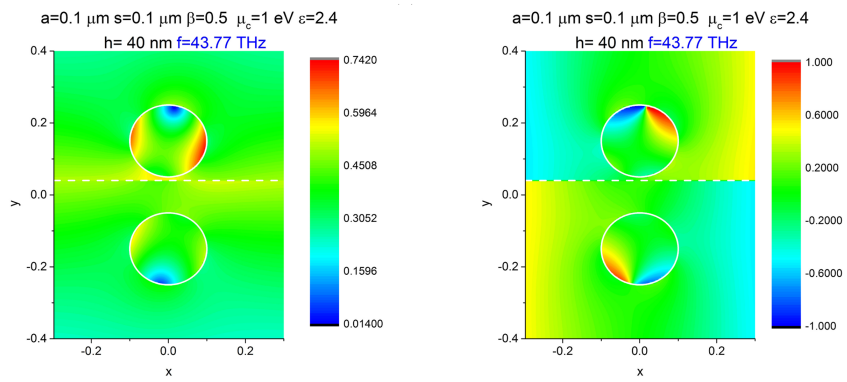

(c) 43.77 THz

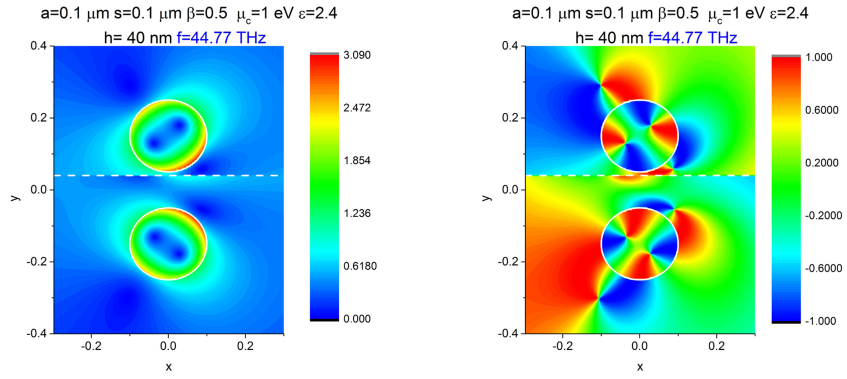

(d) 44.77 THz

Fig. 5. In-resonance near magnetic field magnitude (left) and phase (right) patterns of twin dielectric nanowires covered with graphene with radius $a = 0.1$ μm, the chemical potential $\mu_c = 1$ eV, beam shift $h = 40$ nm, and air gap width $s = 0.1$ μm. (a) 30.16 THz; (b) 32.3 THz; (c) 43.77 THz; (d) 44.77 THz.

While the fabrication of thinner wires seems to be realistic, the largest reported value so far of graphene's chemical potential is only 1 eV (still, larger values can become realistic in future). Indeed, the computations made for $a = 100$ nm with $\mu_c = 0.5$ eV and 1 eV (see the plots in Fig. 3 and Fig. 4, respectively), reveal the same but sharper resonances on the still unresolved mode doublets *EO-OO*, both in SCS and ACS. However, now a shift of the beam trajectory triggers the excitation of new resonances on the unresolved mode doublets *EE-OE*, which remained dark if the beam was not shifted. Such resonances are associated with the "supermodes" of twin wires, whose symmetry is orthogonal to the not-shifted beam field [Eq. (2)]. This is exactly the same effect that we are looking for to be used in BPM design. Note that if a sizably larger, say, 10 eV, chemical potential could be realized, then the mentioned new peaks become impressively larger and sharper (not shown here).

An earlier similar effect was found in the nanosize models of BPMs built on twin high-refractive-index dielectric wires [24] and twin silver nanotubes [26]. Note that in [24,26] the range corresponded to the visible-light frequencies, while what we discuss here takes place at one order lower IR frequencies. Of course, in the circular dielectric wires, a modulated beam of particles can excite the resonances on the WG modes as well (slightly perturbed by the presence of graphene cover); however, for the wire radius taken here they become visible at the frequencies well above 100 THz.

The near fields, computed in the peaks of SCS for the case of the shifted beam trajectory, are shown in Fig. 5. Here, the left panel in each row corresponds to the field magnitude pattern while the right one corresponds to the field phase pattern. These patterns demonstrate the expected number of the field variations around the wires and support our interpretation of the plasmon-mode resonances as those associated with still unresolved supermode pairs of the y-even (*EE* and *OE*) and y-odd (*EO* and *OO*) classes of symmetry.

5. CONCLUSION

We have analyzed, using a dedicated numerical code based on the reduction of the diffraction-radiation problem to the matrix equation having guaranteed convergence, a 2D model of BPM designed of twin graphene-coated circular dielectric nanowires. This analysis has demonstrated that such a dimer can serve as an infrared-range sensor of the beam shift from prescribed trajectory. If such a shift appears, then new resonances on the formerly dark supermodes start shining in the spectral dependence of the DR. To have these new peaks well resolved, the graphene chemical potential should be rather high, around or above 0.5 eV. Such high values can be achieved with appropriate DC biasing.

Funding. National Research Foundation of Ukraine (NRFU #2020-02-0150).

Acknowledgment. We acknowledge partial financial support by the NFRU and the IEEE Photonics Society in the form of the Graduate Student Scholarship to the first author.

Disclosures. The authors declare no conflicts of interest.

Data Availability. Data underlying the results presented in this paper are not publicly available at this time but may be obtained from the authors upon reasonable request.

REFERENCES

1. T. Low and P. Avouris, "Graphene plasmonics for terahertz to mid-infrared applications," ACS Nano **8**, 1086–1101 (2014).
2. Z. Ullah, G. Witjaksono, I. Nawi, N. Tansu, M. I. Khattak, and M. Junaid, "A review on the development of tunable graphene nanoantennas for terahertz optoelectronic and plasmonic applications," Sensors **20**, 1401 (2020).
3. J. Zhao, X. Liu, W. Qiu, Y. Ma, Y. Huang, J.-X. Wang, K. Qiang, and J.-Q. Pan, "Surface-plasmon-polariton whispering-gallery mode analysis of the graphene monolayer coated InGaAs nanowire cavity," Opt. Express **22**, 5754–5761 (2014).
4. J. P. Liu, X. Zhai, L. L. Wang, H.-J. Li, F. Xie, Q. Lin, and S.-X. Xia, "Analysis of mid-infrared surface plasmon modes in a graphene-based cylindrical hybrid waveguide," Plasmonics **11**, 703–711 (2016).
5. C. Dai, K. Agarwal, H. A. Bechtel, C. Liu, D. Joung, A. Nemilentsau, Q. Su, T. Low, S. J. Koester, and J.-H. Cho, "Hybridized radial and edge coupled 3D plasmon modes in self-assembled graphene nanocylinders," Small **17**, 2100079 (2021).
6. B. Zhu, G. Ren, Y. Yang, Y. Gao, B. Wu, Y. Lian, and J. Wang, "Field enhancement and gradient force in the graphene-coated nanowire pairs," Plasmonics **10**, 839–845 (2015).
7. M. Naserpour, C. J. Zapata-Rodríguez, S. M. Vuković, H. Pashaeiadl, and M. R. Belić, "Tunable invisibility cloaking by using isolated graphene-coated nanowires and dimers," Sci. Rep. **7**, 12186 (2017).
8. M. Cuevas, S. H. Raad, and C. J. Zapata-Rodríguez, "Coupled plasmonic graphene wires: theoretical study including comp ex frequencies and field distributions of bright and dark surface plasmons," J. Opt. Soc. Am. B **37**, 3084–3093 (2020).
9. S. J. Smith and E. M. Purcell, "Visible light from localized surface charges moving across a grating," Phys. Rev. **92**, 1069 (1953).
10. A. I. Nosich, "Diffraction radiation which accompanies the motion of charged particles near an open resonator," Radiophys. Quantum Electron. **24**, 696–701 (1981).
11. L. A. Pazynin and V. G. Sologub, "Radiation of a point charge moving uniformly along the axis of a narrow cylindrical ring," Radiophys. Quantum Electron. **25**, 64–68 (1982).
12. L. A. Pazynin and V. G. Sologub, "Excitation of a cylindrical retarding system of finite length by a modulated flux of charge particles," Radiophys. Quantum Electron. **30**, 376–387 (1987).
13. G. I. Zaginaylov, Y. V. Gandel, and P. V. Turbin, "Modeling of plasma effect on the diffraction radiation of relativistic beam moving over a grating of finite extent," Microwave Opt. Technol. Lett. **16**, 50–54 (1997).
14. M. Castellano, V. A. Verzilov, L. Catani, A. Cianchi, G. Orlandi, and M. Geitz, "Measurements of coherent diffraction radiation and its application for bunch length diagnostics in particle accelerators," Phys. Rev. E **63**, 056501 (2001).
15. A. Nosych, C. Boccard, and M. Gasior, "Electromagnetic simulations of an embedded BPM in collimator jaws," in *European Workshop on Beam Diagnostics and Instrumentation for Particle Accelerators (DIPAC)*, Hamburg, Germany (2011), pp. 71–73.
16. G. Valentino, A. A. Nosych, R. Bruce, M. Gasior, D. Mirarchi, S. Redaelli, B. Salvachua, and D. Wollmann, "Successive approximation algorithm for beam-position-monitor-based LHC collimator alignment," Phys. Rev. Spec. Top. Accel. Beams **17**, 021005 (2014).
17. B. Salvant, O. Aberle, and M. Albert, "Beam induced RF heating in LHC in 2015," in *International Particle Accelerator Conference (IPAC)*, Busan, Republic of Korea (2016), pp. 602–605.
18. L. Bobb, R. Kieffer, T. Lefevre, S. Mazzoni, T. Aumeyr, P. Karataev, M. Billing, J. Conway, and J. Shanks, "Feasibility of diffraction radiation for noninvasive beam diagnostics as characterized in a storage ring," Phys. Rev. Accel. Beams **21**, 03801 (2018).
19. T. Muto, S. Araki, R. Hamatsu, H. Hayano, T. Hirose, P. Karataev, G. Naumenko, A. Potylitsyn, and J. Urakawa, "Observation of incoherent diffraction radiation from a single-edge target in the visible-light region," Phys. Rev. Lett. **90**, 104801 (2003).
20. P. Karataev, S. Araki, R. Hamatsu, H. Hayano, T. Muto, G. Naumenko, A. Potylitsyn, N. Terunuma, and J. Urakawa, "Beam-size measurement with optical diffraction radiation at KEK accelerator test facility," Phys. Rev. Lett. **93**, 244802 (2004).

21. M. Bergamaschi, A. Aryshev, P. Karataev, R. Kieffer, T. Lefevre, S. Mazzoni, N. Terunuma, and R. Yang, "Noninvasive micrometer-scale particle-beam size measurement using optical diffraction radiation in the ultraviolet wavelength range," Phys. Rev. Appl. **13**, 014041 (2020).
22. N. Talebi, "Interaction of electron beams with optical nanostructures and metamaterials: from coherent photon sources towards shaping the wave function," J. Opt. **19**, 103001 (2017).
23. D. O. Yevtushenko, S. V. Dukhopelnykov, and A. I. Nosich, "Modeling of optical diffraction radiation from a dielectric and a silver nanowire excited by a modulated electron beam," Opt. Quantum. Electron. **51**, 29 (2019).
24. D. O. Yevtushenko, S. V. Dukhopelnykov, and A. I. Nosich, "Electron beam excitation of supermodes of a photonic molecule built on twin high refractive index dielectric nanowires," J. Appl. Phys. **125**, 223102 (2019).
25. D. O. Yevtushenko and S. V. Dukhopelnykov, "Visible light from modulated electron beam moving between twin circular silver nanowires forming plasmonic photonic molecule," J. Opt. **22**, 025002 (2020).
26. D. O. Herasymova, S. V. Dukhopelnykov, M. Lucido, and A. I. Nosich, "Optical sensing of electron-beam position with twin silver nanotube antenna tuned to hybrid surface plasmon resonance," IEEE J. Sel. Top. Quantum Electron. **27**, 4601008 (2021).
27. D. Y. Sergeeva and A. A. Tishchenko, "On the polarizability of a cluster of interacting particles in polarization radiation," Phys. Atomic Nuclei **83**, 1489–1492 (2020).
28. E. A. Velichko, "Evaluation of a dielectric microtube with a graphene cover as a refractive-index sensor in the THz range," J. Opt. **18**, 035008 (2016).
29. H.-J. Li, L.-L. Wang, J.-Q. Liu, Z.-R. Huang, B. Sun, and X. Zhai, "Investigation of the graphene based planar plasmonic filters," Appl. Phys. Lett. **103**, 211104 (2013).
30. H.-J. Li, L.-L. Wang, B. Sun, Z.-R. Huang, and X. Zhai, "Tunable mid-infrared plasmonic band-pass filter based on a single graphene sheet with cavities," J. Appl. Phys. **116**, 224505 (2014).
31. H. Li, C. Ji, Y. Ren, J. Hu, M. Qin, and L. Wang, "Investigation of multi-band plasmonic metamaterial perfect absorbers based on graphene ribbons by the phase-coupled method," Carbon **141**, 481–487 (2019).
32. S. V. Dukhopelnikov, R. Sauleau, and A. I. Nosich, "Integral equation analysis of terahertz backscattering from circular dielectric rod with partial graphene cover," IEEE J. Quantum Electron. **56**, 8500208 (2020).
33. S. V. Dukhopelnikov, M. Lucido, and A. I. Nosich, "Circular dielectric rod with conformal strip of graphene as tunable terahertz antenna: interplay of inverse electromagnetic jet, whispering gallery and plasmon effects," IEEE J. Sel. Top. Quantum Electron. **27**, 4600908 (2021).
34. G. W. Hanson, "Dyadic Green's functions and guided surface waves for a surface conductivity model of graphene," J. Appl. Phys. **103**, 064302 (2008).
35. G. O. Olaofe, "Scattering by two cylinders," Radio Sci. **5**, 1351–1360 (1970).
36. D. Felbacq, G. Tayeb, and D. Maystre, "Scattering by a random set of parallel cylinders," J. Opt. Soc. Am. A **11**, 2526–2538 (1994).
37. V. I. Fesenko, V. I. Shcherbinin, and V. R. Tuz, "Multiple invisibility regions induced by symmetry breaking in a trimer of subwavelength graphene-coated nanowires," J. Opt. Soc. Am. A **35**, 1760–1768 (2018).
38. F. Frezza, F. Mangini, and N. Tedeschi, "Introduction to electromagnetic scattering. Part II. Tutorial," J. Opt. Soc. Am. A **37**, 1300–1315 (2020).
39. E. A. Velichko and D. M. Natarov, "Localized versus delocalized surface plasmons: dual nature of resonances on a silver circular wire and a silver tube of large diameter," J. Opt. **20**, 075002 (2018).
40. E. I. Smotrova, A. I. Nosich, T. M. Benson, and P. Sewell, "Optical coupling of whispering-gallery modes in two identical microdisks and its effect on photonic molecule lasing," IEEE J. Sel. Top. Quantum Electron. **12**, 78–85 (2006).
41. D. O. Herasymova and S. V. Dukhopelnykov, "Full-wave numerical modeling of beam position monitors on silver nanowires and nanotubes: analysis of solution convergence," in *International Conference on Electronics and Nanotechnologies (ELNANO-2020)*, Kyiv, Ukraine (2020), pp. 77–80.